Spatial Intelligence Through Combined Sensing, Using Computer Vision and on Board Electromagnetics Modelling to Enhance Signals Intelligence and Situational Awareness

T. G. Pelham, MIEEE, MIET
[1]Dept. of Electrical Engineering – University of Bristol, United Kingdom

t.g.pelham@bristol.ac.uk

ABSTRACT

As the cost of antenna arrays continues to decrease, there is an emerging opportunity for the combination of flexible electromagnetics models, modular and distributed antenna array design, and computer vision to provide enhancements to the situational awareness of platform operators. Combining computer vision, efficient electromagnetics modelling and radio channel measurements can provide a consistent understanding of the local environment for improved signals intelligence and situational awareness using commercial off the shelf (COTS) mobile AI modules. In this paper, an open source electromagnetics model is presented for simulation of distributed antenna arrays on complex platforms (LyceanEM), and the use of computer vision based spatial mapping (DepthAI) to populate a channel model for improved direction finding using a 4x4 MIMO spatial intelligence node powered by an Nvidia Orin AGX. A combination of simulated and measured signals will be used to demonstrate the initial workflow for onboard environment mapping, characterisation, and direction finding within the node. The influence of the channel model on signals localisation accuracy will be examined and the fusion of radio and vision based spatial characterisation.

1.0 INTRODUCTION

The drive for increased data rates, energy efficiency, and spectrum efficiency within the arena of mobile communications has had a significant effect on the availability and cost of antenna arrays, including the emergence of RF systems on a chip which can provide significant bandwidth and edge processing to handle the data stream in order to carry out multiple input multiple output (MIMO) processing [1]. However, the deployment of capable antenna arrays onto complex structures is not without drawbacks in a congested electromagnetic environment. When mobile communications are considered, there is a emphasis placed upon different MIMO schemes which depend upon polling the channel information regularly to adjust the beamforming to deliver each users datastream without a prioi knowledge of the physical channel for radio propagation. This is exacerbated in more dynamic environments when there is a requirement for accurate signals intelligence which can be provided by onboard antenna arrays designed to provide angle of arrivals for different signals. In order to provide both increased energy efficiency mobile communications, and accurate and timely signals intelligence there is a requirement to provide some form of channel model which allows the operator to relate signals into the environment. When this is combined with the increasing availability of low cost options for spatial mapping [2], there is an attractive opportunity for a combination of spatial mapping and onboard electromagnetics modelling to transform the signals intelligence workflow.

2.0 SPATIAL MAPPING FOR LOCALISATION AND CHARACTERISATION

2.1 Measurement Setup

In order to investigate the effectiveness of computer vision based environment mapping for the creation of ad hoc radio channel models, two different measurement scenarios were setup Anechoic Chamber. The first is a purely line of sight measurement to test the ability of the spatial intelligence node to localise the LoRa beacon with no other factors involved. The second placed a aluminium 30cm square cast tooling plate into the chamber in order to provide a source of multipath. The two measurement scenarios were included in the digital twin of the anechoic chamber in order to allow modelling on "clean" dataset. This can then be compared to the depth mapping provided by the onboard spatial mapping cameras.

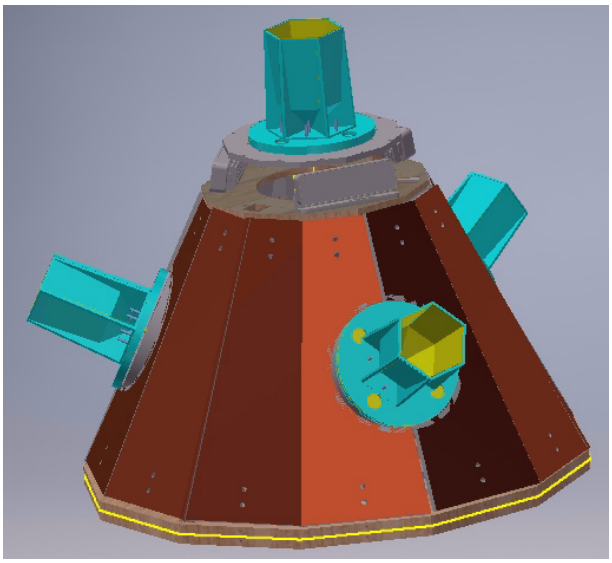

Figure 1: Spatial intelligence node with 4 omnidirectional antennas and DepthAI S2-W cameras.

In order to investigate spatial localisation, RF Fingerprinting, and spatial mapping, the spatial intelligence node is equipped with two USRP B210 software defined radios [3], three DepthAI S2-W cameras [2], [4], and an Nvidia Orin AGX Developer kit, to provide the onboard compute required to run the spatial mapping and channel model process. To provide the test signals, a LoPy 4 module on a Pytrack 2.0 X carrier board was used in beacon mode. The LoPy 4 module was connected to an antenna within the anechoic chamber on a rotator mount, allowing for precise movement of the signal source within the chamber.

The spacing of the omnidirectional antennas around the spatial intelligence node is intended to allow for a combination of spatial discrimination and polarisation discrimination. The top antenna providing omnidirectional vertically polarised coverage, and the other three providing a mixture of horizontal and vertical, with horizontal dominating. In each measurement set the B210s were setup to sampling 15MHz, centred at 867MHz.

A challenging aspect of using the DepthAI cameras within the anechoic chamber is the need to provide suitable lighting for the cameras to be able to image the chamber without oversaturation. The Oak-D S2-W cameras used in these measurements using two sperate monochrome cameras with fisheye lenses in order to perform disparity mapping to obtain a depth profile. This is the combined with the images from a central 4K RGB camera in order to produce a RGB point map, which is then merged onboard the Orin. The Oak-D S2-W stereo cameras have a baseline distance (separation) of 7.5cm which provides an ideal sensing range of 40cm to 6m. The theoretical maximum distance which can be sensed using this camera set is ~10m, which in

principle allows the full anechoic chamber to be mapped. In practice, the forward camera which should be able to provide a spatial map of the beacon and rotator is not able to cope with the lighting conditions within the chamber, even with the addition of a floodlight behind the spatial intelligence node in order to provide bright and even illumination within the chamber. These issues can be seen clearly in Figure 3, which shows the depth map picking up the position and color of the reflector plate and stand, but increasing distortion as the shadowing increases "behind" the spatial intelligence node, where the floodlight does not provide consistent illumination.

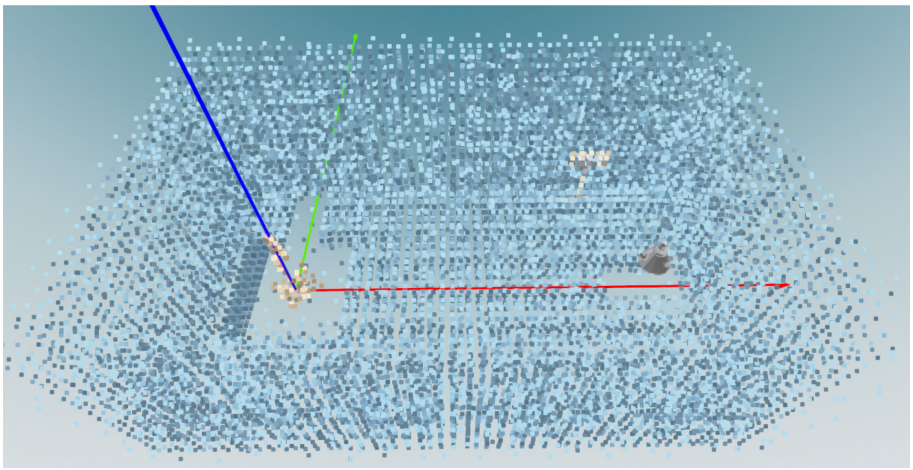

Figure 2: Point cloud for multipath scenario with anechoic chamber with rotator aligned to 45 degrees.

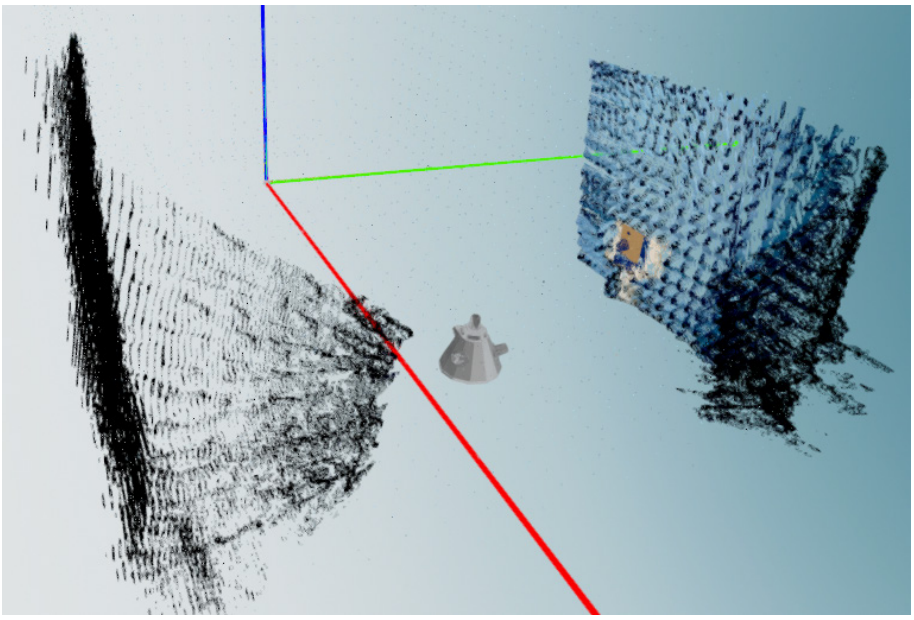

Figure 3: DepthAI point cloud from onboard cameras, with recorded position of reflector and chamber axes.

2.2 Modelling Setup

The onboard modelling used to turn the spatial map into a radio channel model is LyceanEM, and open source electromagnetics model implemented in Python. LyceanEM uses Nvidia's CUDA acceleration in order to provide frequency and time domain channel models. Originally designed for rapid virtual prototyping of antenna arrays, the current model architecture is based upon discrete raytracing, rather than shooting and bouncing rays, and has some limitations which are to be addressed in future releases [6], [7]. The fundamental issues for channel models in complex environments is that materials in the computational environment are limited to perfect absorbers and perfect electrical conductors. Despite this, at 24GHz, it has demonstrated an agreement with measurement on the order of -69dB rms error [8].

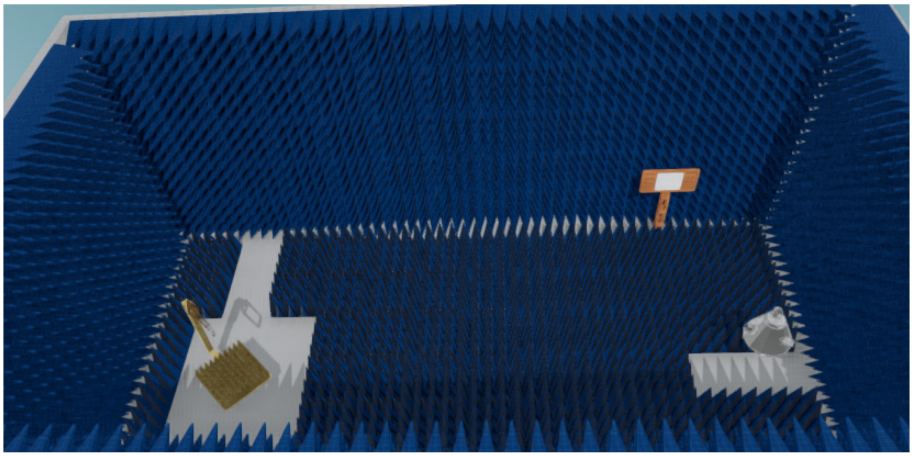

Figure 4: Rendering of multipath scenario within anechoic chamber with rotator aligned to 45 degrees.

3.0 RESULTS

3.1 Measurements

The depth mapping provided by the DepthAI cameras produces a close agreement with the true position of the scattering plate, as shown in Figure 3. This is highly dependant upon the lighting conditions, which could be reduced if an active camera using structure light was used, or more consistent lighting via a dedicated light rig. This does provide a basis for machine learning based approaches to tag the points which are likely to be reflectors, based upon semantic segmentation to break up the depth map of the environment into different objects, and predicting their properties.

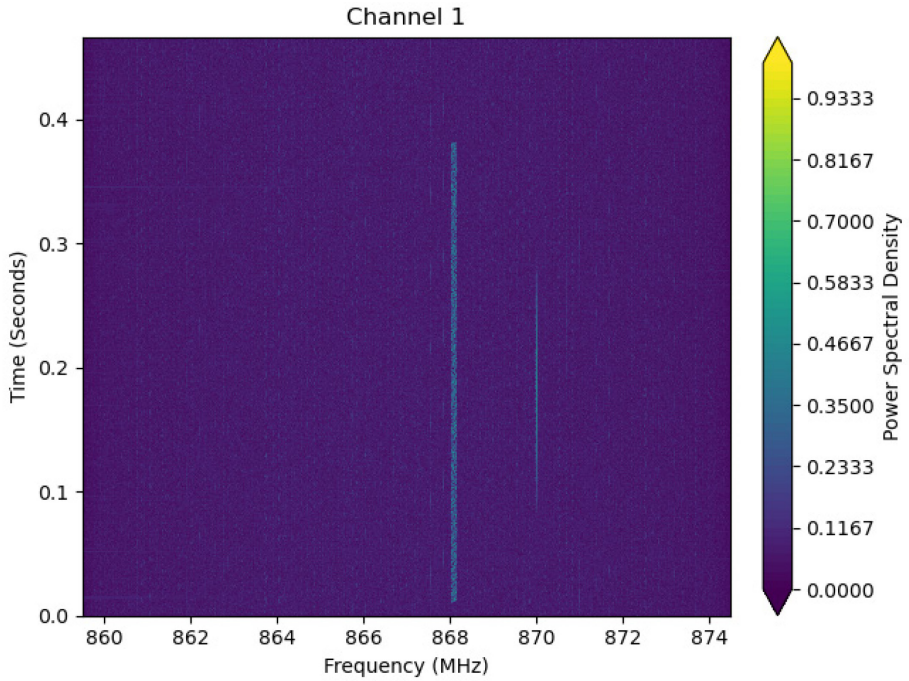

Figure 5: Example frequency - Time plot for one of the LoRa waveforms captured.

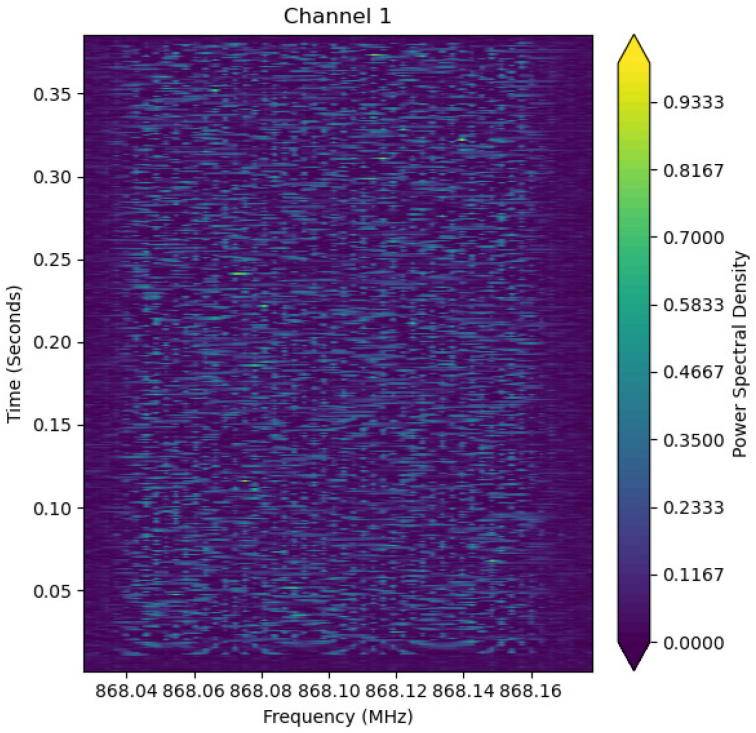

Figure 6: "Zoomed In" view of the waveform shown in Figure 5.

The frequency upchirps at the start of the waveform in Figure 6, with a spreading factor of 7, and a signal bandwidth of 125kHz. However, at the sampling rate of 15MHz, it is difficult to discern the packet structure within the waveform, while it is recoverable. Figure 5 also shows one of the persistence noise sources within the chamber while carrying out the measurement series at 870MHz. The captured waveforms were processed in the frequency domain using paired sum and difference beamforming to form angle of arrival spectrums in azimuth and elevation. This method was used because the time and frequency alignment between the two radios was not sufficient to allow for true 4x4 MIMO operation, and hence each radio was used standalone, with one radio connected to the "top" and "forward" antennas, selective in elevation, and one radio connected to the "left" and "right" antennas. Despite this the azimuth error was low despite the wide beamwidth of the antennas used (91 degrees), while the elevation error was high. It is interesting to note that when the scattering plate is introduced to the chamber the error in estimated angle of arrival decreases in both azimuth and elevation. This is thought to be due to the scattering plate introducing an asymmetry into the propagation channel. This can be clearly seen in Figure 7, with a higher power illumination on the wall of the chamber compared at the location of the scattering plate.

Table 1: Measured angle of arrival maximum in azimuth and elevation.

Beacon Position	Estimated Azimuth	Error	Estimated Elevation	Error
Line of Sight Only				
-45°	-174	9	-47	53
0°	-174	6	-45	51
45°	179	4	-47	53
Scattering Plate Included				
-45°	177	0	-38	44
0°	174	6	-37	43
45°	-178	0.5	-31	37

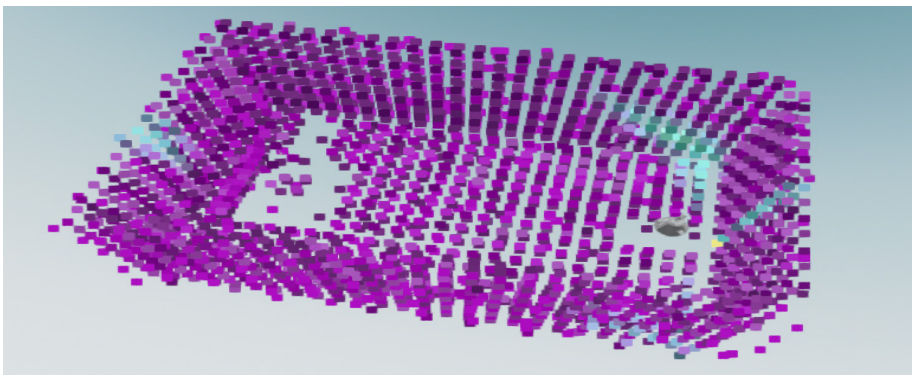

Figure 7: Spatial map of the anechoic chamber for scattering plate with beacon rotated to -45 degrees.

3.2 Modelling

The modelled channel, and angle of arrivals shown in Table 2 are a marked difference from the measured results due to the dominance of the line of sight component. When the scattering plate is included the accuracy of the channel model in terms of the angles of arrival is not significantly effected, while the measured spatial discrimination improves with the inclusion of the scattering plate.

Table 2: Modelled angle of arrival maximum in azimuth and elevation.

Beacon Position	Estimated Azimuth	Error	Estimated Elevation	Error
Line of Sight Only				
-45°	180	3	1	5
0°	180	0	1	5
45°	180	3	1	5
Scattering Plate Included				
-45°	177	0	1	5
0°	177	3	1	5
45°	176	7	1	5

This is likely due to the idealised electric current sources used for the antenna patterns for the spatial intelligence node within the channel model. The actual antenna patterns when measured are omnidirectional, but are not as linearly polarised as an ideal pattern, and have some slightly difference response in elevation.

3.3 Comparison

The onboard channel model provided similar accuracy estimations of the angle of arrival to that of the measured sum and difference beamforming. However, in order to do this the channel model included the exact position of the antenna. This demonstrates the ability of the channel model to replicate propagation conditions inside the anechoic chamber at 868MHz, which is low enough frequency to present challenges to some ray tracing approaches. It is likely that the agreement between model and measurement would be closer if modelled or measured antenna patterns were used each of the spatial intelligence nodes channels. This approach is equivalent to the spatial intelligence node guessing a transmitter position, then checking the received signal and angle of arrival spectrum produced by the channel model against the measured angle of arrival spectrum. This is suitable for the development of generative adversarial networks (GAN) in order to generate spatially relevant machine learning training datasets, which presents and attractive approach to solving the location encoding of existing methods of machine learning datasets which include channel information.

4.0 CONCLUSIONS

This initial series of measurements has provided an introduction to the use of onboard channel modelling to predict the propagation environment. In these initial measurements, a digital twin of the anechoic chamber as created in order to isolate the model errors from those propagated by noisy spatial mapping, and the spatial map created was included for reference and to discuss the current shortcomings. Despite the issues, the information provided by the spatial map is promising for future machine learning approaches to populating channel models for dynamic environments. Combined with the DepthAI capability to track pedestrians in real time using each cameras onboard processing, this is a promising avenue for future investigate. Given the wide beamwidth of the antennas used the azimuth errors of the measured system were, low, and the modelled channel produced similar results. This can likely be improved by introducing more realistic antenna patterns as sources within LyceanEM, which is on the development roadmap for this open source software.

5.0 REFERENCES

[1] C. Horne, N. J. Peters, and M. A. Ritchie, "Classification of LoRa Signals With Real-Time Validation Using the Xilinx Radio Frequency System-on-Chip," IEEE Access, vol. 11, pp. 26211–26223, 2023, doi: 10.1109/ACCESS.2023.3252170.

[2] luxonis, "{DepthAI}: Embedded Machine learning and Computer vision api." 2020, [Online]. Available: https://luxonis.com/.

[3] R. Zitouni and L. George, "Output power analysis of a software defined radio device," in 2016 IEEE Radio and Antenna Days of the Indian Ocean (RADIO), Oct. 2016, pp. 1–2, doi: 10.1109/RADIO.2016.7771996.

[4] luxonis, "{OAK-D}: Stereo camera with Edge AI." 2020, [Online]. Available: https://luxonis.com/.

[5] T. G. Pelham, A. L. Freire, G. Hilton, and M. Beach, "Polarimetric Scattering with Discrete Raytracing for OTA Analysis," 2021, doi: 10.23919/EuCAP51087.2021.9410981.

[6] T. G. Pelham, "Rapid antenna and array analysis for virtual prototyping," Int. Conf. Radar Syst. (RADAR 2022), pp. 278–282, 2022, doi: 10.1049/ICP.2022.2330.

[7] T. G. Pelham, G. Hilton, E. Mellios, and R. Lewis, "Conformal {Antenna} {Array} {Design} {Using} {Aperture} {Synthesis} and {On}-{Platform} {Modeling}," IEEE Access, vol. 9, pp. 60880–60890, 2021, doi: 10.1109/ACCESS.2021.3074317.

[8] T. G. Pelham, A. L. Freire, G. Hilton, and M. Beach, "Polarimetric Scattering with Discrete Raytracing for OTA Analysis," in 15th European Conference on Antennas and Propagation, EuCAP 2021, 2021, pp. 1–4, doi: 10.23919/EuCAP51087.2021.9410981.